Microsyst Technol (2007) 13:61–70
DOI 10.1007/s00542-006-0257-1

TECHNICAL PAPER

Analysis of the dynamic behaviour of a torsional micro-mirror

Dong-Ming Sun · Wei Dong · Cai-Xia Liu · Wei-You Chen · Michael Kraft

Received: 20 April 2006 / Accepted: 21 August 2006 / Published online: 20 September 2006
© Springer-Verlag 2006

Abstract In this paper, the results of the dynamic pull-in voltage characteristics of a micro-mirror using electrostatic actuation are analyzed. Based on torsional dynamic theory, appropriate equations are developed that allowed to give insight into the actuating voltage, switching time and other dynamic parameters. The analytical results are discussed in detail without and with considering air squeeze film damping, respectively. This is equivalent to assuming the mirror is operated in vacuum or at ambient pressure. When the effect of the damping is considered, the movement trajectory of the cantilever beam is changed, and the calculated results of the pull-in voltage and switching time are considerably different compared to those without considering damping. Therefore, the effect of the air squeeze film damping is an important factor in the design and fabrication of micro-electro-mechanical systems. Finally, the experimental results in the air environment are discussed and compared to the theoretical analysis.

Keywords MEMS · Micro-mirror · Electrostatic actuation · Dynamic · Air squeeze film damping

D.-M. Sun (✉) · W. Dong · C.-X. Liu · W.-Y. Chen (✉)
College of Electronic Science and Engineering,
State Key Laboratory on Integrated Optoelectronics,
Jilin University, Changchun 130012, China
e-mail: dongmingsun2008@yahoo.com.cn

W.-Y. Chen
e-mail: chenwy@mail.jl.cn

W. DongChangchun Institute of Optics,
Fine Mechanics and Physics,
Chinese Academy of Sciences,
Changchun 130021, China

M. Kraft
Nanoscale Systems Integration Group,
School of Electronics and Computer Science,
Southampton University,
Southampton SO17 1BJ, UK
e-mail: mk1@ecs.soton.ac.uk

1 Introduction

In recent years, many micro-electro-mechanical systems (MEMS) devices and components, including sensors and actuators, have been developed as this technology is maturing rapidly. Several actuation methods have been investigated, such as electromagnetic (Maekoba et al. 2001), electrostatic (Rosa et al. 2004), piezoelectric (Huang et al. 2004) and electrothermal (Syms et al. 2002). However, electrostatic actuation is the most widely utilized method for the design of MEMS. Due to the dimensional constraints of MEMS devices, the air squeeze film damping is an important parameter for their performance, design and control. Therefore, the effect of the squeeze film damping on the dynamics of microstructures has been studied by several researchers (Starr 1990; Andrews et al. 1993; Nayfeh et al. 2004). Furthermore, for smaller devices, when electrodes and a movable part are physically coming into contact, the coupling effects of the gas rarefaction and surface roughness on the dynamical characteristics have been investigated. Another important effect for the dynamic behavior of many MEMS devices is the electrostatic pull-in phenomenon which is basically due to the nonlinear characteristics of electrostatic forces. These are always attractive as they depend on the square of the applied voltage, and the inverse of the distance between the

electrodes squared. The mechanical restoring force of the microbeam cannot keep up with the electrostatic force for higher actuating voltages, which can lead to the upper electrode collapsing into the lower electrode; the so-called 'pull-in' phenomenon (Chowdhury et al. 2005). In the following discussion static and dynamic pull-in effects are distinguished; the former is solely due to the electrostatic action. The inertia and damping terms are neglected and the variation of the voltage is considered slow enough so that equilibrium is obtained at any time by the static force components (Rocha et al. 2004). Zhang et al. (2001) and Xiao et al. (2001) analyzed the quasi-static characteristics of electrostatic actuation for a torsion micromirror. The analysis of the dynamic pull-in phenomenon additionally has to take into account the inertial and damping effects and the influence of external acceleration, which may significantly change the pull-in voltage threshold.

In this paper, the dynamic characteristics are investigated for an electrostatically actuated micro-actuator whose main application is to act as a mirror to steer a light beam. The analytical results are discussed in detail without and with considering air squeeze film damping, respectively. This is equivalent to assuming the mirror is operated in vacuum or at atmospheric pressure. This paper is organized as follows: first, in Sect. 2, based on the micro-mirror model, the torque on the cantilever beam is described and corresponding equations are derived. Furthermore, the theory of torsion dynamics and the solution of the dynamic equation are presented. In Sect. 3, by using these equations, the calculations of dynamic parameters are performed without considering the air squeeze film damping. In Sect. 4, the calculations are discussed with considering the air squeeze film damping, and the experimental results and theoretical analysis are compared and discussed. Finally, conclusions are drawn in Sect. 5 on the basis of the analysis and discussion.

2 Modeling and analysis

Figure 1 shows a schematic diagram of an actuated micro-mirror. It consists of a cantilever beam acting as mirror, a balance beam, torsion beams, and a lower electrode. If operated in air, there is an air squeeze film between the cantilever beam and the lower electrode. The actuation voltage is applied between the cantilever beam and the lower electrode. This voltage creates an electrostatic force that causes a bending angle of the cantilever beam tip. We define the 'switch-off' time T_{off} as the switching time required to move the mirror from the reflection state into the transmission state and the 'switch-on' time T_{on} as the time required to move the mirror from the transmission state into the reflection state. The material properties, geometrical parameters and other required parameters for the analysis of the micro-mirror are listed in Table 1

2.1 Torque on the cantilever beam

2.1.1 *Electrostatic torque*

When an actuating voltage V is applied between the cantilever beam and the lower electrode, an electrostatic force F results. Since the gap between the cantilever beam and substrate is considerably smaller than the electrode area, two assumptions can be made to simplify the calculation: (1) the distribution of the electrostatic field is uniform along the y-axis parallel to the torsion beams; (2) the shape of the field is represented by an arc and any fringing field is neglected. At x on the cantilever beam, the length of the arc can be calculated as $(H/\sin\theta - x)\theta$ By integrating the electrostatic torque over the length of the cantilever beam, $x = [0, L_{\mathrm{C}}]$, an equation for the electrostatic torque M_{E} can be derived as (Toshiyoshi and Fujita 1996)

$$M_{\mathrm{E}} = \frac{\varepsilon_0}{2} V^2 w \int_0^{L_{\mathrm{C}}} \frac{x}{\left(\frac{H}{\sin\theta} - x\right)^2 \theta^2} \mathrm{d}x = \frac{\varepsilon_0 V^2 w}{2\theta^2} \times \left(\ln \frac{H - L_{\mathrm{C}} \sin\theta}{H} + \frac{L_{\mathrm{C}} \sin\theta}{H - L_{\mathrm{C}} \sin\theta} \right) \quad (1)$$

where ε_0 is the dielectric constant in free space, of which the value is taken to be 8.85×10^{-12} F/m, θ is the torsion angle of the cantilever beam.

2.1.2 *Restoring torque*

When the cantilever beam moves down under the action of the electrostatic force, it is evident that the torsion beam undergoes both torsion and bending. In the following analysis, the bending and torsion forces are uncoupled and treated separately. The equation for torsional spring constant K_θ is (Lee et al. 1999)

$$K_\theta = 2 \times \frac{Gab^3}{3L_{\mathrm{T}}} \left[1 - \frac{192}{\pi^5} \frac{b}{a} \tan h \left(\frac{\pi a}{2b} \right) \right] \qquad (a \geq b) \quad (2)$$

where G is the shear modulus of silicon, of which the value is taken to be 0.52×10^{11} Pa for (100) silicon. The spring constant for bending K_{b} is given as

$$K_{\mathrm{b}} = \frac{Eb}{2} \left(\frac{a}{L_{\mathrm{T}}} \right)^3 \quad (3)$$

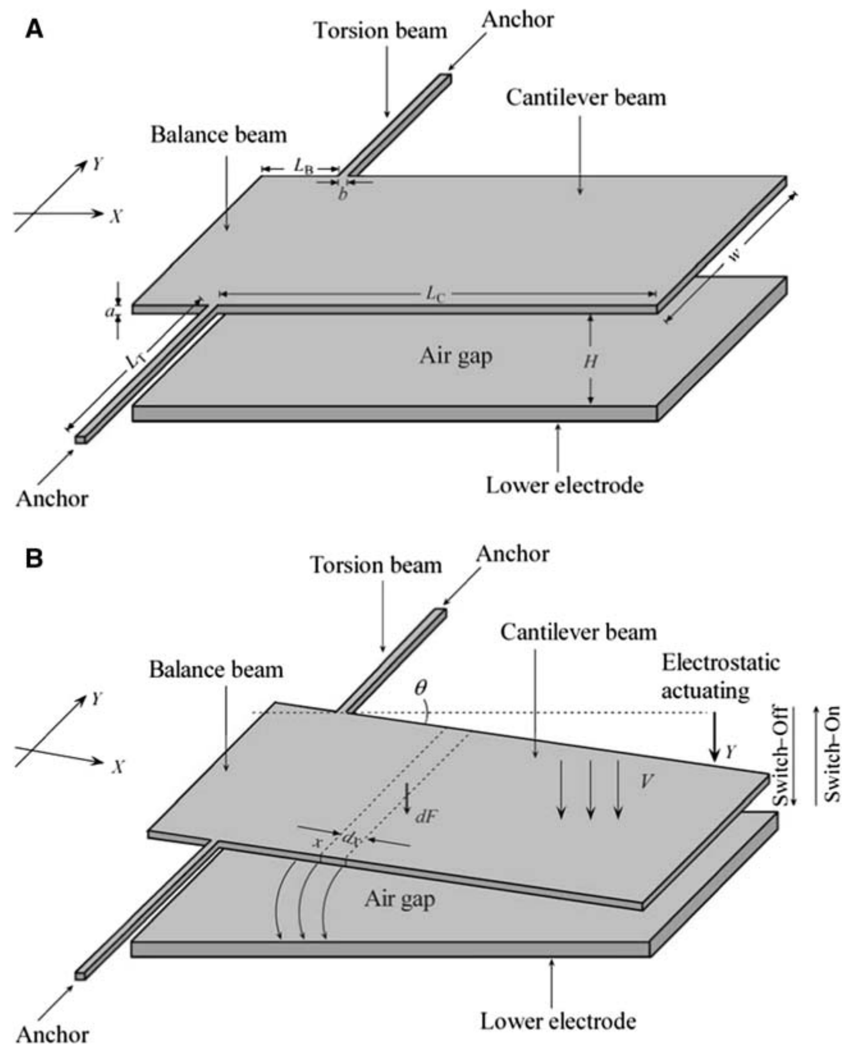

Fig. 1 The electrostatically actuated micro-mirror under consideration: **a** without applied actuating voltage; **b** with applied actuating voltage

where E is the Young's modulus of silicon, of which the value is taken to be 1.30×10^{11} Pa. It can be seen that K_θ is proportional to $1/L_\mathrm{T}$ and K_b is proportional to $1/L_\mathrm{T}^3$ thus for the torsional micro-mirror, the bending distortion becomes important and notable only when the length of the torsion beam is very long. For the micro-mirror considered in this paper, the bending distortion of the torsion beam is so small that it can be safely neglected. This can be inferred from Fig. 2, which shows the relationship between the displacement of the cantilever beam tip Y and the actuating voltage V. In this figure, the bending of the beam is plotted without considering the twisting of the torsion beam. We can see that the torsion beam bends down considerably only for larger actuating voltage. In the subsequent sections of the paper the actuating voltage is assumed to be less than 50 V which provides enough force to twist the torsion beam. The displacement Y is very small in this range and can safely be neglected. Therefore, the torsion beam twists but does not bend when the mirror moves down. This is also reason why a design using a micro-mirror based on torsional movement can reduce the actuating voltage considerably compared to a design based on linear motion

The restoring torque M_T of the torsion beam can be expressed as a function of the torsion angle θ

$$M_\mathrm{T} = K_\theta \theta = 2 \times \frac{Gab^3\theta}{3L_\mathrm{T}}\left[1 - \frac{192}{\pi^5}\frac{b}{a}\tan h\left(\frac{\pi a}{2b}\right)\right] \quad (4)$$

2.1.3 Gravity torque

The cantilever beam also experiences a small rotational displacement by torque due to gravity, and the balance beam will counteract and reduce this displacement by the part to the left of the torsion beam, also due to gravity (see Fig. 1). The gravity force is acting orthogonal to the xy-plane. The gravity torque

Table 1 Parameters required for the analysis of the micro-mirror

Parameter	Variable	Value (unit)
Material properties		
Density of silicon	ρ	2.33×10^{3} kg m^{-3}
Shear modulus of silicon	G	0.52×10^{11} Pa
Young's modulus of silicon	E	1.30×10^{11} Pa
Viscosity coefficient of air (1 atm, 298 K)	η	1.79×10^{-5} Pa s
Acceleration of gravity	g	9.8 m s^{-2}
Dielectric constant of vacuum	ε_0	8.854×10^{-12} F/m
Device properties		
Length of the torsion beam	L_T	700 μm
Width of the torsion beam	b	12 μm
Length of the cantilever beam	L_C	1,900 μm
Width of the cantilever beam	w	1,000 μm
Thickness of the upper electrode	a	12 μm
Length of the balance beam	L_B	300 μm
Distance between the cantilever beam and lower electrode	H	55 μm
Other required parameters for the analysis		
Torsion angle of the cantilever beam	θ	
Pull-in torsion angle of the cantilever beam	θ_{pin}	
Actuating voltage between the cantilever beam and lower electrode	V	
Pull-in voltage	V_{pin}	
Electrostatic force	F	
Electrostatic torque	M_E	
Spring constant for torsion of the torsion beam	K_θ	
Spring constant for bending of the torsion beam	K_b	
Restoring torque	M_T	
Gravity torque of the cantilever beam	M_G	
Gravity torque of the balance beam	M_B	
Damping pressure caused by the damping of the air squeeze-film	P	
Spacing between the upper and lower electrodes	h	
Squeeze film damping torque	M_D	
Squeeze film damping coefficient	C	
Moment of inertia of the rigid body	I	
Actuator capacitance	Q	
Angular acceleration	β	
Angular velocity	ω	
'Switch-off' time	T_{off}	
'Switch-on' time	T_{on}	

of the cantilever beam M_G and that of the balance beam M_B are given by, respectively

$$M_G = \int_0^{L_C} \rho awgx \cos\theta \, dx = \frac{\rho awg \cos\theta L_C^2}{2} \quad (5)$$

$$M_B = \int_0^{L_B} \rho awgx \cos\theta \, dx = \frac{\rho awg \cos\theta L_B^2}{2} \quad (6)$$

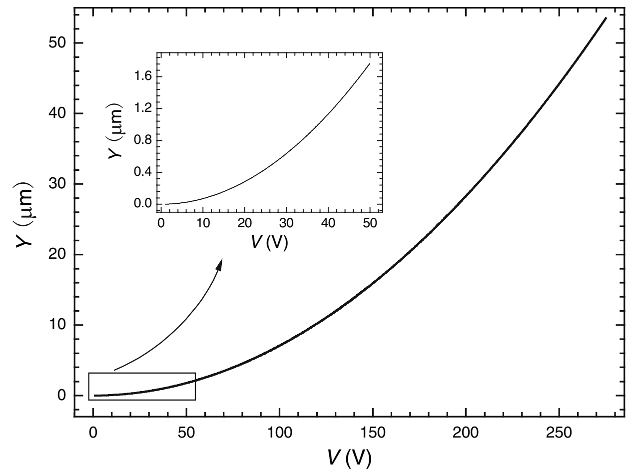

Fig. 2 Relationship between the displacement of the cantilever beam tip Y and actuating voltage V when only considering the effect of bending

where ρ is the density of silicon, and g is the acceleration of gravity.

2.1.4 *Squeeze film damping torque*

The damping is mainly due to a small air gap that exists between the cantilever beam and the substrate. In the movement of the cantilever beam, the air is squeezed out or sucked in through the edges of the plates. The squeeze film damping torque originates from the pressure distribution on the cantilever beam surface. Since the gap H is smaller than the plates extent, that is $H \ll L_C$ and w, the aspect ratio of the micro-mirror is large. On the assumptions that the air behaves under the ideal gas law and the system is isothermal, the damping of the air squeeze film can be analyzed by using the following Reynolds' equation (Pan et al. 1998)

$$\frac{\partial}{\partial x}\left(h^3 \frac{\partial P}{\partial x}\right) + \frac{\partial}{\partial y}\left(h^3 \frac{\partial P}{\partial y}\right) = 12\eta \frac{\partial h}{\partial t} \quad (7)$$

where P is the damping pressure caused by the damping of the air squeeze-film, and η is the viscosity coefficient of air at room temperature, of which the value is taken to be 1.79×10^{-5} Pa s.

Since the cantilever beam rotates around the torsion beam (y-axis), the distribution of the air pressure P is uniform in the direction of the y-axis:

$$\frac{\partial P}{\partial y} = 0 \quad (8)$$

For small torsion angles, $\sin\theta$ can be approximated by θ, thus the spacing h can be expressed as

$$h = \left(\frac{H}{\sin\theta} - x\right)\theta \approx H - x\theta \tag{9}$$

Substituting Eqs. (8) and (9) into Eq. (7), we obtain the following relationship:

$$\frac{\partial^2 P}{\partial x^2} + \frac{3\theta}{x\theta - H}\frac{\partial P}{\partial x} - \frac{12\eta}{(H - x\theta)^3}\frac{\mathrm{d}h}{\mathrm{d}t} = 0 \tag{10}$$

Based on the following boundary conditions, $x = 0$, $P = 0$ and $x = L_C$, $P = 0$, the damping pressure P can be expressed from Eq. (10) as

$$P = \frac{12\eta x(x - L_C)}{(2H - L_C\theta)(H - x\theta)^2}\frac{\mathrm{d}h}{\mathrm{d}t} \tag{11}$$

The equation for the squeeze film damping torque M_D can be derived as

$$M_D = \int_0^{L_C} \frac{12\eta x(x - L_C)}{(2H - L_C\theta)(H - x\theta)^2}\frac{\mathrm{d}h}{\mathrm{d}t} xw\,\mathrm{d}x \tag{12}$$

From Eq. (9) follows that $\mathrm{d}h/\mathrm{d}t = -\dot{\theta}x$ this can be substituted into Eq. (12) and by defining the squeeze film damping coefficient as $C = M_D\big/\dot{\theta}$ we obtain

$$C = \frac{2w\eta}{(2H - L_C\theta)\theta^5}\left[L_C\theta\left(L_C^2\theta^2 - 24H^2 + 6HL_C\theta\right) + 6H^2(4H - 3L_C\theta)\ln\frac{H}{H - L_C\theta}\right] \tag{13}$$

2.2 Static characteristics

For studying the static characteristics of the pull-in phenomena, the inertia and damping can be neglected. The cantilever beam is driven by the actions of the electrostatic actuation and elastic restoring force. However, as the initial gap decreases, the electrostatic force increases much faster than the linear restoring force, except if the increased variation of the voltage is slow enough so that equilibrium is at any time obtained. At a specific gap, this equilibrium is not longer valid and pull-in occurs. Therefore, we can conduct the pull-in analysis for the specific gap where the electrostatic force and restoring force are balanced (Degani et al. 1998; Zhang et al. 2001).

At equilibrium, $M_E = M_T$, thus

$$\frac{1}{2}\frac{\partial Q}{\partial\theta}V^2 = K\theta \tag{14}$$

where Q is the actuator capacitance. Differentiating Eq. (14) with respect to θ yields

$$K = \frac{1}{2}\frac{\partial^2 Q}{\partial\theta^2}V^2 \tag{15}$$

By substituting Eq. (15) into Eq. (14), we obtain the equation describing the pull-in phenomenon,

$$\frac{\partial^2 Q}{\partial\theta^2}\Big|_{\theta=\theta_{\mathrm{pin}}} - \frac{1}{\theta_{\mathrm{pin}}}\frac{\partial Q}{\partial\theta}\Big|_{\theta=\theta_{\mathrm{pin}}}\Big| = 0 \tag{16}$$

The pull-in voltage can be derived by combining Eqs. (14) and (16),

$$V_{\mathrm{pin}} = \sqrt{\frac{2K}{\frac{\partial^2 Q}{\partial^2\theta}\big|_{\theta=\theta_{\mathrm{pin}}}}} \tag{17}$$

For a torsional actuator, the capacitance is given by

$$Q = \frac{\varepsilon_0 w}{\theta}\ln\frac{H}{H - L_C\theta} \tag{18}$$

Substituting Eq. (18) into Eqs. (16) and (17), the pull-in deflective angle and pull-in voltage are expressed as, respectively

$$\theta_{\mathrm{pin}} = 0.44\,\tan^{-1}\left(\frac{H}{L_C}\right) \tag{19}$$

$$V_{\mathrm{pin}} = \sqrt{\frac{0.83KH^3}{\varepsilon_0 L_C^3 w}} \tag{20}$$

The pull-in angle is independent of the pull-in voltage or the spring constant K, and therefore, θ_{pin} is a constant of the structure. From Eq. (2) we can get the torsional spring constant of the torsion beam, which contributes to the pull-in voltage. Based on the structural parameters listed in Table 1, we can calculate the following results as $\theta_{\mathrm{pin}} = 0.73°$ (i.e. the displacement of the cantilever beam tip is 24.2 μm) and $V_{\mathrm{pin}} = 31.4$ V.

2.3 Theory of torsion dynamics

In order to derive analytical expressions for the 'switch-on' and 'switch-off' times, the dynamic equations for a rigid body have to be solved. This also allows to determine the expressions for the angular acceleration β and angular velocity ω. The equation of motion is:

$$M_{\rm E} + M_{\rm G} - M_{\rm T} - M_{\rm B} = I\beta + C\omega \tag{21}$$

where $C\omega$ is the air squeeze film damping torque, $I = \rho(L_{\rm C} + L_{\rm B})^3 wa/3$ is the moment of inertia of the rigid body. Defining $M(\theta) = M_{\rm E} + M_{\rm G} - M_{\rm T} - M_{\rm B}$, Eq. (21) can be written as

$$M(\theta) = I\beta + C\omega \tag{22}$$

Since $M(\theta)$ is a complex nonlinear function of θ, a numerical method must be used to solve Eq. (22). We divide the switching time T into n intervals, i.e. $\Delta T = T/n$ and the torsion angle is denoted as θ_i in the i-th interval.

$$\omega_i = \dot{\theta}_i = \frac{\theta_{i+1} - \theta_{i-1}}{2\Delta T} \tag{23}$$

$$\beta_i = \ddot{\theta}_i = \frac{\theta_{i+1} - 2\theta_i + \theta_{i-1}}{\Delta T^2} \tag{24}$$

Substituting Eqs. (23) and (24) into Eq. (22), we can obtain an iterative equation for θ_{i+1}, θ_i and θ_{i-1} as follows

$$\theta_{i+1} = \frac{\left[2I\theta_i + \left(\frac{C(\theta_i)\Delta T}{2} - I\right)\theta_{i-1} + M(\theta_i)\Delta T^2\right]}{I + \frac{C(\theta_i)\Delta T}{2}} \tag{25}$$

where $C(\theta_i)$ and $M(\theta_i)$ are functions of θ. By using the initial conditions $\theta_0 = 0$ and assuming a small enough value for $\Delta T = 10^{-8}$ s, then θ_1 can be calculated from Eq. (21). According to Eq. (25), we can obtain the value for θ for every time interval. The values of $T_{\rm off}$, $T_{\rm on}$, β and ω can be calculated from the iterative process, thus the movement of the cantilever beam is described for all times.

3 Calculated results—without considering air squeeze film damping

In order to clearly demonstrate the importance of the air squeeze film damping on the micro-mirror, we give the analytical results without and with considering the air squeeze film damping, respectively. This is equivalent to operating the device in vacuum or in ambient air, respectively.

Figure 3 shows the ratio of the electrostatic torque $M_{\rm E}$ and the restoring torque $M_{\rm T}$ as a function of the beam tip displacement Y for different actuating voltages. It can be seen that $M_{\rm E}$ is less than $M_{\rm T}$ in the middle part of the movement, which implies a negative angular acceleration. When the actuating voltage is 27.2 V, at point A on the curve, the deflection of the beam tip is about 36.5 μm, and the electrostatic force is equal to the restoring force. At this point, it can be seen from Fig. 4 that the angular acceleration β is zero.

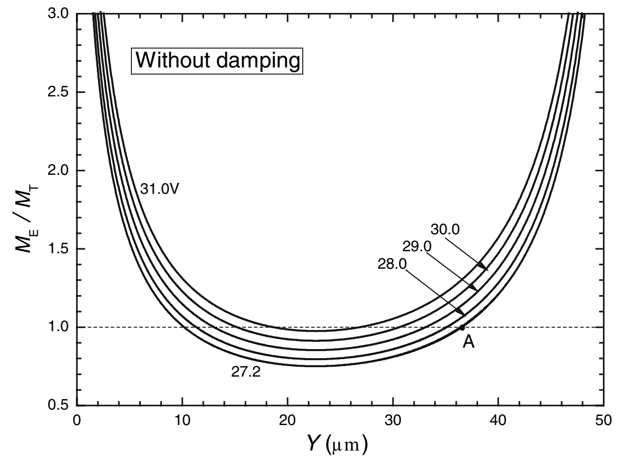

Fig. 3 Relationship between the ratio of the electrostatic torque, $M_{\rm E}$ and the torque from the torsion beam, M_T as a function of the beam tip displacement Y for different actuating voltages

Figure 4 shows the relationship between the angular acceleration β and the displacement of the cantilever beam tip Y for different actuating voltages. For the actuating voltages considered here, β decreases at first and then increases in the second half of the movement trajectory. We should note that for smaller actuating voltages (less than 30.0 V), in a certain range of the beam tip displacement Y, the value of β is negative. For an actuating voltage of 30.0 V the value of β is zero and the displacement of Y is about 25.7 μm (point B in the diagram). The dashed curve shows the calculated results without considering the gravity torque (for

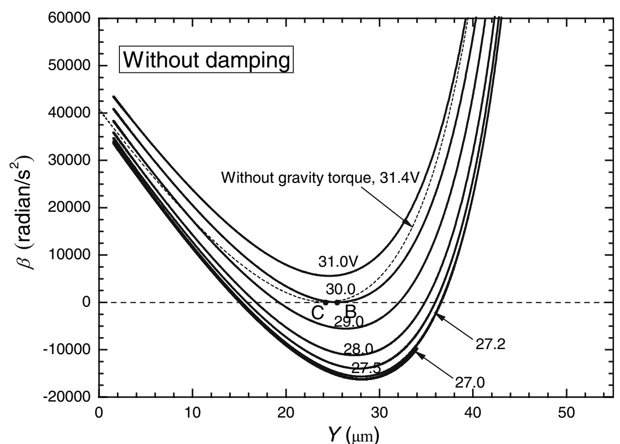

Fig. 4 Relationship between the angular acceleration β and the displacement of the cantilever beam tip Y for different actuating voltages (without air damping)

V =31.4 V). At point C on the curve, β is zero again and Y is about 24.2 μm. These results coincide with the values calculated for the static characteristics for the pull-in phenomena. However, zero angular acceleration at point C means only that the sum of all of forces is zero, and hence point C is not the pull-in position, as it is for the static case. The following discussions show that the movement of the cantilever beam will continue due to the inertia effect, consequently the pull-in voltage will be decreased and the pull-in angle will be increased.

Figure 5 shows the relationship between the angular velocity ω and the beam tip displacement Y for different actuating voltages. We can see that first ω increases with an increase in Y, but then exhibits a distinctive behavior depending on the actuating voltages. For actuating voltages smaller than 27.2 V, the cantilever beam will not move down completely but vibrates periodically. When the actuating voltage is larger than 27.2 V, the minimum of ω is positive, and the cantilever beam snaps down. For actuating voltages larger than 30.0 V, ω increases continuously; this implies that the angular acceleration β is positive at all times (see Fig. 4). The value of ω is zero at point D on the curve, therefore we can deduce that the pull-in voltage of the micro-mirror is about 27.2 V, and the pull-in position is about 36.5 μm. These results are significantly different to the static characteristics analysis. The inertia effect has an important effect on the movement of the cantilever beam. Since the spacing h decreases, the electrostatic force increases much faster than the linear restoring force. During the final stage of the cantilever movement the angular velocity of the beam increases rapidly, therefore, it snaps down to the lower electrode

Figure 6 shows the trajectory of the cantilever beam as a function of time for different actuating voltages. The 'switch-off' time T_{off} can directly be read from the diagram for a displacement of about 50.0 μm. As expected, it is found that T_{off} decreases with an increase in the actuating voltage. When the actuating voltage increases from 27.2 to 31.0 V, T_{off} decreases from 3.5 to 1.3 ms.

4 Calculated results—with considering air squeeze film damping

When the effect of the air squeeze film damping is considered, the movement trajectory of the cantilever beam is changed, and the calculated results of the pull-in voltage and switching time are considerably different compared to those without considering the air damping. The cantilever beam cannot move down completely when the actuating voltage is smaller. Therefore, the pull-in voltage of the micro-mirror is increased, and the following analysis yields that the pull-in voltage is about 31.0 V when air damping is considered. This change is entirely due to the effect of the air damping. For smaller actuation voltages (25–35 V), the cantilever beam cannot move down completely when damping is considered. For larger voltages (35–50 V), the pull-in phenomena cannot be studied and analyzed without considering damping effects. Therefore, different actuating voltages have to be considered in the following.

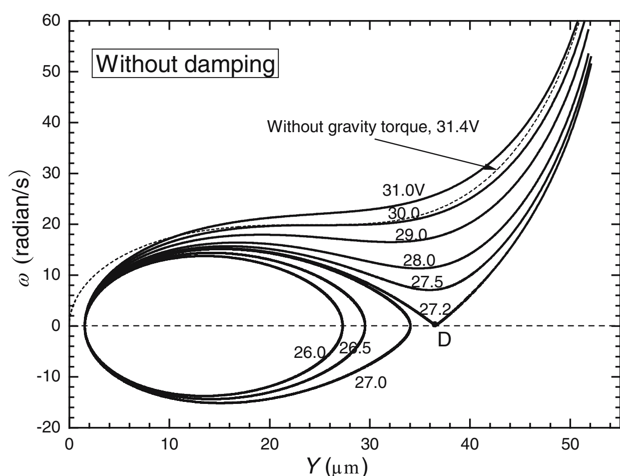

Fig. 5 Relationship between the angular velocity ω and the beam tip displacement for different actuating voltages (without air damping)

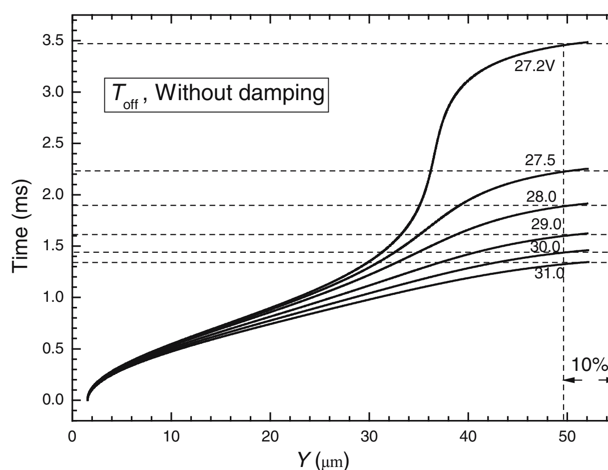

Fig. 6 Trajectory of the cantilever beam as a function of time for different actuating voltages (without air damping)

Figure 7 shows the relationship of the ratios of the torque due to damping to the electrostatic torque (M_D/M_E) and the restoring torque of the torsion beam (M_D/M_T), respectively, versus the displacement Y for different actuating voltages. We can see that M_D/M_E and M_D/M_T are larger in the initial and later stages of the movement, and the magnitude of M_D is comparable to that of M_E and M_T.

Figure 8 shows the relationship between the angular velocity ω and the displacement Y for different actuating voltages. The distance denoted by the symbol Δ shows the initial displacement of the cantilever beam tip caused by the gravity torque M_G of the cantilever beam. We can see that ω increases as V increases. For voltages within a range from 31.0 to 50.0 V, as Y increases, first ω increases rapidly, then decreases gradually, and then increases in the second half of the movement. When the actuating voltage is 30.0 V, the cantilever beam cannot snap down, but stops moving at a certain point F on the curve. At this point, the displacement of the cantilever beam tip is about 24.0 μm, and the value of ω is zero. At the displacement of 24.0 μm, the value of the angular acceleration β is also zero, as shown at the point G in Fig. 9. This indicates that when the actuating voltage is less than 30.0 V, the cantilever beam moves down incompletely, and stops at a certain location. The cantilever beam is balanced at this point under the actions of the electrostatic torque, restoring torque and gravity torque. When the actuating voltage is more than 31.0 V, the cantilever beam can snap down and contact the lower electrode. However, the higher actuating voltage also leads to a considerably different switching time. The switching time will be shorter because of the larger angular velocity for a larger actuating voltage. Due to the increased electrostatic torque, the cantilever beam can continue to move beyond the point E (the minimum of the angular velocity), and eventually snaps down. Thus, the pull-in voltage of the micro-mirror is about 31.0 V when considering damping, and the pull-in position is about 24.5 μm (i.e. $\theta_{pin} = 0.74°$). These results are in good agreement with the analysis of static characteristics. When the actuating voltage is 31.0 V, the angular velocity ω decreases gradually by the action of the air damping and ω is close to zero at a displacement of 24.5 μm. Furthermore, the action of the air damping is weakened with a decrease in the angular velocity ω. Therefore, we can say that the movement trajectory of the cantilever beam is similar to the equilibrium state of the static characteristics. Thus, we obtain similar values of θ_{pin} and V_{pin} compared to the analysis of the static characteristics.

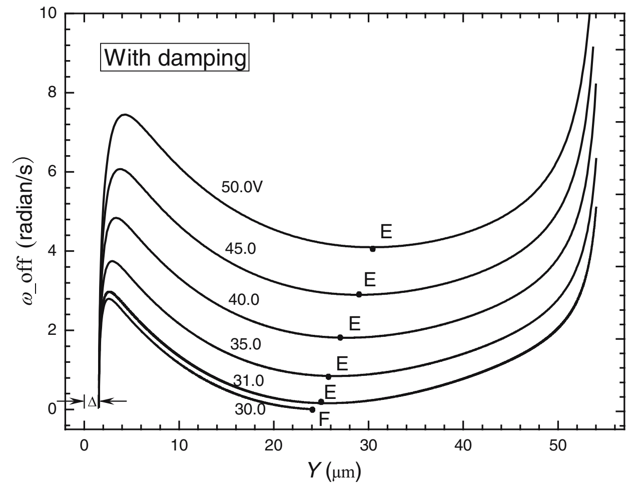

Fig. 8 Relationship between the angular velocity ω and the displacement of the cantilever beam tip Y for different actuating voltages (with air damping)

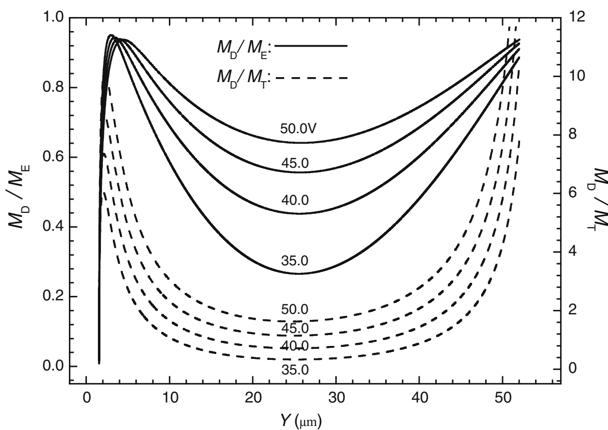

Fig. 7 Relationship of M_D/M_E and M_D/M_T versus the displacement of the cantilever beam tip Y

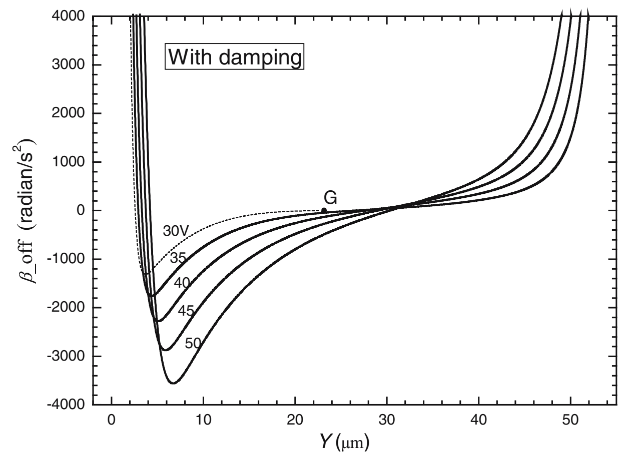

Fig. 9 Relationship between the angular acceleration β and the displacement of the cantilever beam tip Y for different actuating voltages for 'switch-off' (with air damping)

The relationship of the angular acceleration β and the angular velocity ω versus the displacement Y for ‘switch-on’ are illustrated in Fig. 10. We can see that ω increases at first and then decreases with a decrease of Y. The values of β and ω are closer to zero at the end of movement. This means that the cantilever beam can keep balance and eventually stops moving.

Figure 11 shows the trajectory of the cantilever beam as a function of time for different actuating voltages with considering the air squeeze film damping. T_{off} decreases with an increase in the actuating voltage V. When V is 35.0 V, T_{off} is about 19.0 ms; however, for V = 50.0 V, T_{off} is only about 5.0 ms. The curve shows that the angular velocity ω is not zero at the final point of the movement because the slope of curve is not zero at the end of movement for ‘Switch-off’, and the cantilever beam snaps down and comes into contact with the lower electrode. However, for ‘Switch-on’, T_{on} is about 14.0 ms, and the angular velocity ω is closer to zero at the end of the curve, therefore the cantilever beam can stop at the end of the movement.

Experimental measurements in air have been carried out for the micro-mirror and were reported in detail in reference (Sun et al. 2005). The deflection angle of the cantilever beam and the switching time can be investigated by an optical technique using a CCD camera. The applied actuating voltage V is 50.0 V in the experiment. Here, some experimental results of the measurement are compared with the analytical results presented in this paper. The switching time T_{off} is 5.0 ms (theoretical result), which is more than the experimental result (4.8 ms); and the switching time T_{on} is 14.0 ms (theoretical result), which is also more than the experimental result (12.5 ms). The deviation between the measurement results and theoretical ones is less than 10%. It is envisaged that there are some reasons contributed to this deviation besides the observation error. In the theoretical analysis, the effect of the fringing fields is ignored and there are several assumptions when the behavior of the air is governed by the Reynolds’ equation. However, the above two reasons only result in little error, the more errors come from the experimental process. Firstly, the sharp of the torsion beam is not perfect by the process of reaction ion etching (RIE), and the roughness of torsion beam can influence the performance of the micro-mirror markedly. Secondly, in the assembly process of the electrodes, the distance between the cantilever beam and lower electrode may be increased by the infiltration of gluewater. Thirdly, the cantilever beam is somewhat deformed by the electrostatic force after it has snapped to the lower electrode, thus the torsion angle is increased. Therefore, the measured torsion angle is expected to be larger than that of the theoretical analysis, for which the beam has been assumed as completely rigid. However, so far experimental data has only been obtained for operation of the micro-mirror operating in air, further testing is currently carried out to validate the analytical model at different levels of low pressure.

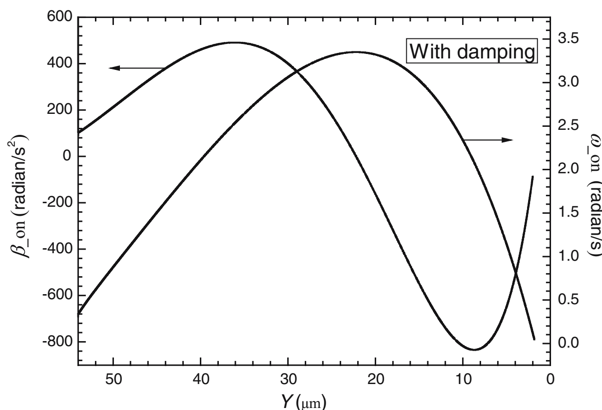

Fig. 10 Relationship of the angular acceleration β and the angular velocity ω versus the displacement of the cantilever beam tip Y for ‘Switch-on’ (with air damping)

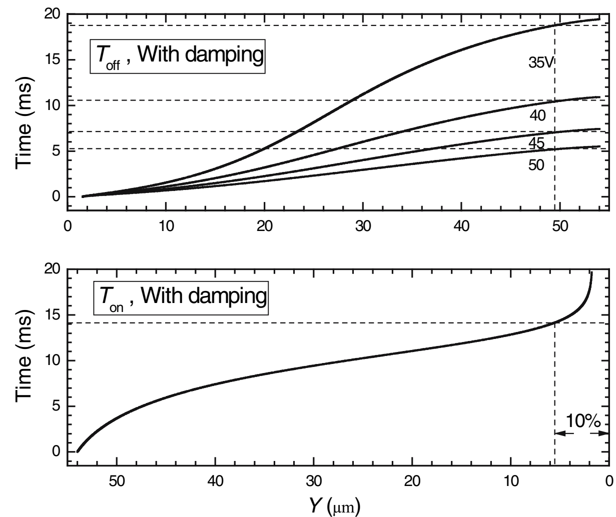

Fig. 11 Trajectory of the cantilever beam as a function of time for different actuating voltages (with air damping)

5 Conclusion

In this paper, an approach is presented for studying the dynamic response of an electrostatically actuated micro-mirror. For the static characteristics of the pull-in phenomena, the calculated pull-in voltage is 31.4 V and the pull-in deflection of the cantilever tip is

24.2 μm. The analytical results are discussed in detail without and with considering the air squeeze film damping, respectively. For the dynamic case these parameters are considerably different due to the influence of inertial effects. Without considering the damping, i.e. operating the device in vacuum, the pull-in deflection is about 36.5 μm and $V_{\mathrm{pin}} = 27.2$ V; with considering the damping, i.e operating the device in air, the pull-in deflection is about 24.5 μm and $V_{\mathrm{pin}} = 31.0$ V. Furthermore, as expected, the switching time increases when air damping is considered. Finally, results obtained by measurements on the micro-mirror are discussed, and it is shown that the experimental results in the air environment are in good agreement with the theoretical analysis of the switching time with considering the air damping. It can be concluded that the air squeeze film damping plays a very important role on the movement of the cantilever beam. If different viscosity coefficients of air are used by operating the device at different pressure, the characteristics of the devices can be varied considerably.

Acknowledgments The authors wish to express their gratitude to the National Research and Development Plan for High Technology of China (the project number of 863 Plan is 2002AA312023), The National Natural Science Foundation of China (the project number is 69937019) and The Graduate Innovation Foundation of Jilin University (the project number is 501038) for their generous support of this work.

References

Andrews M, Harris I, Turner G (1993) A comparison of squeeze-film theory with measurements on a microstructure. Sens Actuators A 36:79–87

Chowdhury S, Ahmadi M, Miller WC (2005) A closed-form model for the pull-in voltage of electrostatically actuated cantilever beams. J Micromech Microeng 15:756–763

Degani O, Socher E, Lipson A et al (1998) Pull-in study of an electrostatic torsion microactuator. J Microelectromech Syst 4:373–379

Huang C, Lin YY, Tang TA (2004) Study on the tip-deflection of a piezoelectric bimorph cantilever in the static state. J Micromech Microeng 14:530–534

Lee SS, Huang LS, Kim CJ et al (1999) Free-space fiber-optic switches based on MEMS vertical torsion mirrors. J Lightwave Technol 17:7–13

Maekoba H, helin P, Reyne G et al (2001) Self-aligned vertical mirror and V-grooves applied to an optical-switch: modeling and optimization of bi-stable operation by electromagnetic actuation. Sens Actuators A 87:172–178

Nayfeh AH, Younis MI (2004) A new approach to the modeling and simulation of flexible microstructures under the effect of squeeze-film damping. J Micromech Microeng 14:170–181

Pan F, Kubby J, Peeters E et al (1998) Squeeze film damping effect on the dynamic response of a MEMS torsion mirror. J Micromech Microeng 8:200–208

Rocha LA, Cretu E, Wolffenbuttel RF (2004) Behavioural analysis of the pull-in dynamic transition. J Micromech Microeng 14:S37–42

Rosa MA, Bruyker DD, Volkel AR et al (2004) A novel external electrode configuration for the electrostatic actuation of MEMS based devices. J Micromech Microeng 14:446–451

Starr JB (1990) Squeeze-film damping in solid-state accelerometers. IEEE Solid-State Sensors and Actuators Workshop, pp 44–47

Sun DM, Dong W, Wang GD et al (2005) Study of a 2 × 2 MOEMS optical switch with electrostatic actuating. Sens Actuators A 120:249–256

Syms RRA (2002) Long-travel electrothermally driven resonant cantilever microactuators. J Micromech Microeng 12:211–218

Toshiyoshi H, Fujita H (1996) Electrostatic micro torsion mirrors for an optical switch matrix. J Microelectromech Syst 4:231–237

Xiao ZX, Wu XT, Peng WY et al (2001) An angle-based design approach for rectangular electrostatic torsion actuators. J Microelectromech Syst 4:561–568

Zhang XM, Chau FS, Quan C et al (2001) A study of the static characteristics of a torsional micromirror. Sens Actuators A 90:73–81